

Mg²⁺ Binds to the Surface of Thymidylate Synthase and Affects Hydride Transfer at the Interior Active Site

Zhen Wang,^{†,⊥} Paul J. Sapienza,[‡] Thelma Abeysinghe,[†] Calvin Luzum,^{†,#} Andrew L. Lee,[‡] Janet S. Finer-Moore,^{||} Robert M. Stroud,^{||} and Amnon Kohen^{*,†}

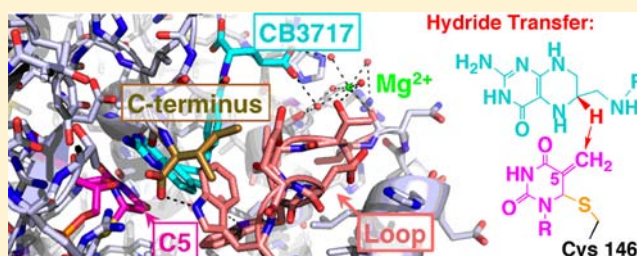
[†]Department of Chemistry, University of Iowa, Iowa City, Iowa 52242, United States

[‡]Division of Chemical Biology and Medicinal Chemistry, UNC Eshelman School of Pharmacy, University of North Carolina at Chapel Hill, Chapel Hill, North Carolina 27599, United States

^{||}Department of Biochemistry and Biophysics, University of California, San Francisco, California 94158, United States

S Supporting Information

ABSTRACT: Thymidylate synthase (TSase) produces the sole intracellular de novo source of thymidine (i.e., the DNA base T) and thus is a common target for antibiotic and anticancer drugs. Mg²⁺ has been reported to affect TSase activity, but the mechanism of this interaction has not been investigated. Here we show that Mg²⁺ binds to the surface of *Escherichia coli* TSase and affects the kinetics of hydride transfer at the interior active site (16 Å away). Examination of the crystal structures identifies a Mg²⁺ near the glutamyl moiety of the folate cofactor, providing the first structural evidence for Mg²⁺ binding to TSase. The kinetics and NMR relaxation experiments suggest that the weak binding of Mg²⁺ to the protein surface stabilizes the closed conformation of the ternary enzyme complex and reduces the entropy of activation on the hydride transfer step. Mg²⁺ accelerates the hydride transfer by ~7-fold but does not affect the magnitude or temperature dependence of the intrinsic kinetic isotope effect. These results suggest that Mg²⁺ facilitates the protein motions that bring the hydride donor and acceptor together, but it does not change the tunneling ready state of the hydride transfer. These findings highlight how variations in cellular Mg²⁺ concentration can modulate enzyme activity through long-range interactions in the protein, rather than binding at the active site. The interaction of Mg²⁺ with the glutamyl tail of the folate cofactor and nonconserved residues of bacterial TSase may assist in designing antifolates with polyglutamyl substitutes as species-specific antibiotic drugs.



■ INTRODUCTION

Metal ions are known to stabilize physiologically active conformations of biomolecules by various mechanisms in cells.^{1,2} The divalent magnesium cation (Mg²⁺) is an essential mineral nutrient for all living organisms, which is involved in many cellular functions including energy metabolism, cell growth, and proliferation, etc.³ Owing to the high intracellular magnesium content (i.e., as high as 20 mM),⁴ cells can exploit the transport of Mg²⁺ between organelles to vary its local concentrations and regulate enzyme activities.^{3,5} Previous studies suggested that the intracellular magnesium content reaches its maximum during the S phase of the cell cycle, concomitant with DNA replication.⁶ In exponentially growing *Escherichia coli* B cells, the intracellular concentration of total Mg²⁺ can be higher than 100 mM.^{7,8}

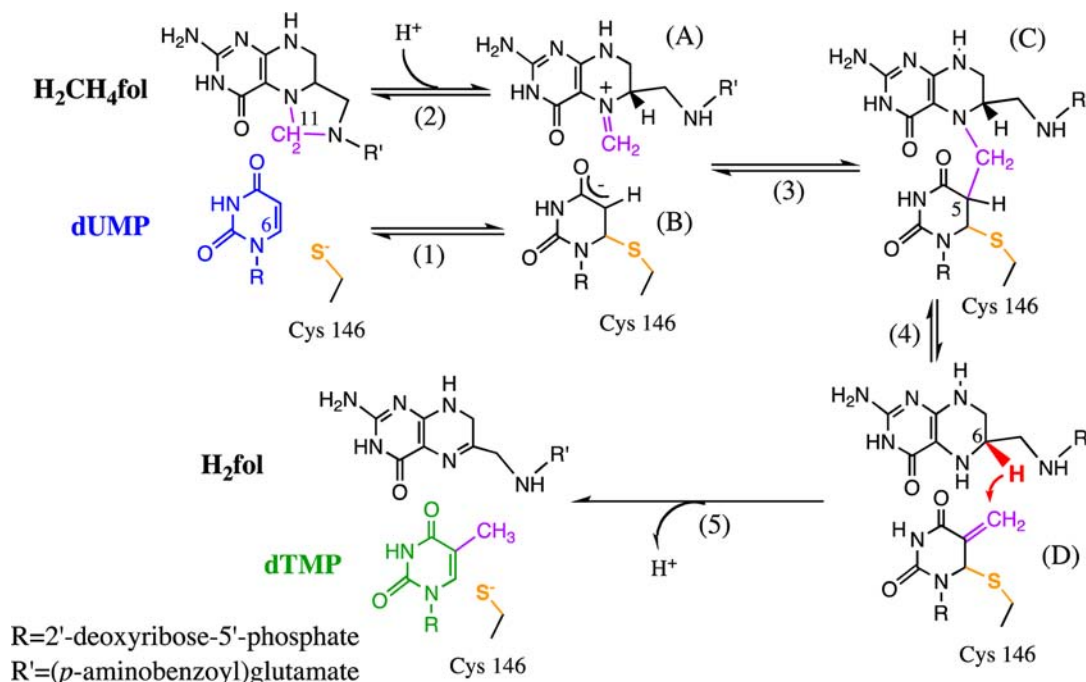
One of the enzymes crucial for DNA replication is thymidylate synthase (TSase), which is one of the most conserved enzymes in evolution.⁹ TSase catalyzes the reductive methylation of 2'-deoxyuridine-5'-monophosphate (dUMP) to form 2'-deoxythymidine-5'-monophosphate (dTMP), using N⁵,N¹⁰-methylene-5,6,7,8-tetrahydrofolate (CH₂H₄fol) as the

cofactor (Scheme 1).¹⁰ This reaction provides the sole de novo source of thymidine (i.e., DNA base T) in the vast majority of organisms, including some bacteria and DNA viruses.^{11–13} TSase is overexpressed in tumor cells to facilitate the faster DNA replication.^{14,15} Consequently, TSase has been an attractive target for both antibiotic and anticancer drugs. Classical drugs that target TSase are structural analogues of either dUMP (e.g., 5-fluorouracil) or CH₂H₄fol (e.g., raltitrexed and other antifolates), which often interfere with the metabolic pathways of nucleosides/nucleotides or folates, leading to toxicity and development of resistance in cells.^{16,17} Therefore, current drug designs focus on avoiding drug resistance and selectively targeting TSase activity in malignant tumor cells or in specific pathogenic species. Careful investigations in the catalytic mechanism of TSase can aid these drug design efforts.^{16,18}

TSase is a homodimer with two active sites, each of which is composed of residues from both protomers, and previous

Received: January 25, 2013

Published: April 23, 2013

Scheme 1. Proposed Mechanism for Thymidylate Synthase¹⁰ (adapted from ref 19 with copyright permission from ACS)^a

^aThis reaction involves a series of chemical conversions (steps 1–5) with multiple intermediates (A–D), and the hydride transfer (red, step 5) is rate limiting for the catalytic turnover.²⁰

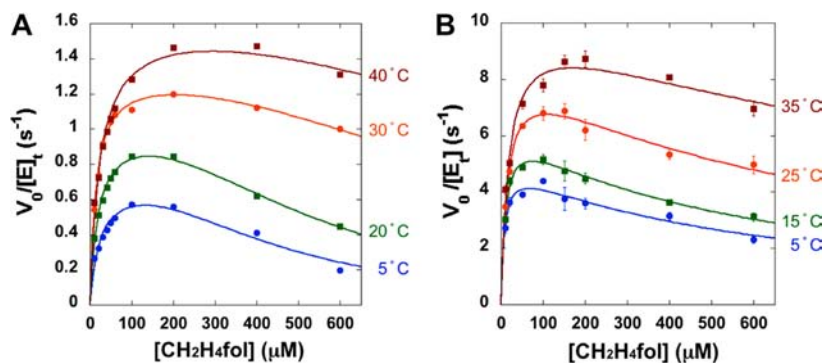


Figure 1. Initial velocity of ecTSase-catalyzed reaction vs concentration of $\text{CH}_2\text{H}_4\text{fol}$, in the (A) absence and (B) presence of 50 mM MgCl_2 . Figure A is adapted from ref 26 with permission from ACS. Detailed data analysis is provided in the Experimental Section.

experiments suggested that TSase has “half-of-the-sites” activity, i.e., only one active site is competent at a time.^{21–23} The large collection of structural and kinetic studies of TSase revealed that protein segments move concertedly throughout the many-step reaction,^{24,25} which has attracted experimental and computational examinations of protein motions that contribute to activation of chemical bonds.^{19,26–32} However, the complex catalytic mechanism of TSase makes it difficult to expose information on the microscopic chemical conversions (e.g., steps 1–5 in Scheme 1). We have measured the kinetic isotope effect (KIE) on the hydride transfer (step 5 in Scheme 1) in *E. coli* TSase (ecTSase),²⁶ which is rate limiting for the catalytic turnover in the absence of Mg^{2+} .²⁰ Similar to H-transfer reactions in many other wild-type enzymes,^{26,33–38} the hydride transfer in ecTSase exhibits a temperature-dependent rate but a temperature-independent KIE. The recently developed Marcus-like model affords an interpretation of those kinetic results, which suggests that protein motions can facilitate an enzymatic H-transfer in three aspects.^{37,39–45} First, conformational

fluctuations of the protein preorganize an electrostatic environment that is favorable for formation of the reactive complexes for the H-transfer step.^{37,46–49} Second, fine-tuning of the conformations of reactive complexes further reorganizes the active site to accommodate structural changes in the substrates going from the reactant state to the tunneling ready state (TRS) of the H-transfer. Third, the fluctuation of donor–acceptor distance (DAD) at the TRS affects the H-tunneling probability. While the DAD fluctuation at TRS determines the magnitude and temperature dependence of the intrinsic KIE, pre- and reorganization affects the rate (and the activation parameters) of the H-transfer and thus the kinetic commitment factor in experimental KIE measurements.^{50,51} To explore the effects of those three categories of protein motions on the hydride transfer, we recently conducted kinetic and structural analysis of a remote mutant of ecTSase, Y209W (9 Å away from the hydride transfer site). This remote mutation affected both the rate and KIE of the hydride transfer through a long-range of

interactions, suggesting that TSase may exploit a “network of coupled motions” to facilitate activation of this C–H bond.¹⁹

Two previous studies reported that Mg^{2+} variably affected TSase activities from different species,^{52,53} but the mechanism of those effects has never been investigated. Here we report detailed kinetic and structural analysis of how Mg^{2+} affects the catalytic mechanism of ecTSase and particularly the hydride transfer step. Our results suggest that, although Mg^{2+} binds weakly to the surface of ecTSase, this interaction stabilizes the productive conformations of both the protein and the bound folate cofactor, thereby accelerating the hydride transfer at the active site (16 Å away).

RESULTS AND DISCUSSIONS

Mg^{2+} Affects the Entropy of Activation on k_{cat} . To investigate the effect of Mg^{2+} on ecTSase activity, we measured the steady-state initial velocities of ecTSase in the absence and presence of 50 mM $MgCl_2$ (i.e., the same concentration used in previous studies).^{52,53} To assess the potential effects of ionic strength on the protein activity, we conducted a control experiment that measured the initial velocities at 25 °C in the absence and presence of 50 mM $CaCl_2$ and found no difference. The cofactor CH_2H_4fol exhibited substrate inhibition at high concentrations in both the absence and presence of Mg^{2+} (Figure 1), which is consistent with its alternate unproductive binding mode in crystal structures.⁵⁴ Based on the analysis of initial velocities (details provided in the Experimental Section), the presence of Mg^{2+} affects the cooperativity of CH_2H_4fol binding in the inhibitory mode, suggesting an effect on the interaction between the protein and folate cofactor.

The analysis of initial velocities above provided the first-order rate constant, k_{cat} , of the reaction at four different temperatures, which were fit to the Eyring equation (eq 1) to evaluate the activation parameters:

$$\ln\left(\frac{k_{cat}}{T}\right) = \frac{-\Delta H^\ddagger}{R} \cdot \left(\frac{1}{T}\right) + \frac{\Delta S^\ddagger}{R} + \ln\left(\frac{k_B}{\hbar}\right) \quad (1)$$

where ΔH^\ddagger is the enthalpy of activation, ΔS^\ddagger is the entropy of activation, T is absolute temperature, and k_B , \hbar , and R are Boltzmann, Planck, and gas constants, respectively. In the temperature range of 5–35 °C, the presence of Mg^{2+} increases k_{cat} by approximately 7-fold (Figure 2). The temperature

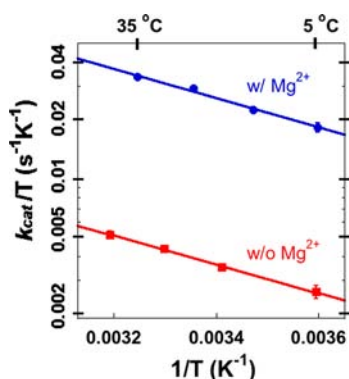


Figure 2. Eyring plots of the initial velocity of ecTSase-catalyzed reaction in the absence (w/o, red) and presence (w/, blue) of 50 mM $MgCl_2$. Mg^{2+} accelerates k_{cat} by ~ 7 -fold, and only affects the entropy of activation by ~ 1 kcal/mol (Table 1).

dependence of k_{cat} is linear in both the absence and presence of Mg^{2+} , suggesting that a single kinetic step is rate limiting for the catalytic turnover in each case. Mg^{2+} reduces the activation free energy and entropy of activation (ΔG^\ddagger and $T\Delta S^\ddagger$ at 25 °C, respectively, see Table 1) of k_{cat} by ~ 1 kcal/mol, while the

Table 1. Activation Parameters from Fitting k_{cat} of ecTSase to the Eyring Equation in the Absence (w/o) and Presence (w/) of 50 mM $MgCl_2$.^a

TSase	ΔH^\ddagger kcal/mol	$-T\Delta S^\ddagger$ at 25 °C kcal/mol	ΔG^\ddagger kcal/mol
w/ Mg^{2+}	3.4 ± 0.2	12.8 ± 0.2	16.2 ± 0.4
w/o Mg^{2+} ^b	3.4 ± 0.1	13.9 ± 0.1	17.3 ± 0.2

^aKIE experiments suggest that the hydride transfer is rate limiting for k_{cat} under both conditions (see text below), thus the steady-state kinetic experiments actually exposed the activation parameters of the hydride transfer step. The values of k_{cat} are presented in Table S1.

^bData are from ref 26.

enthalpy of activation (ΔH^\ddagger) remains the same. These results suggest that Mg^{2+} affects the conformational fluctuations of the active site that constitute the entropic contribution of the catalysis, which is further supported by our NMR relaxation experiments below. We also found that the presence of Mg^{2+} increases the Michaelis constant of dUMP by ~ 5 -fold at 25 °C (Table 2).

Table 2. Michaelis Constants and Dissociation Constants of dUMP and CH_2H_4fol for ecTSase, in the Absence (w/o) and Presence (w/) of 50 mM $MgCl_2$ at 25 °C

	K_M^{dUMP} ^a (μM)	K_d^{dUMP} ^b (μM)	$K_M^{CH_2H_4fol}$ ^a (μM)	$K_d^{CH_2H_4fol}$ ^c (μM)
w/ Mg^{2+}	2.4 ± 0.2	14 ± 2	15 ± 1	8 ± 1
w/o Mg^{2+}	0.5 ± 0.1	8.5 ± 0.9	17 ± 2	17 ± 2

^aMeasured by steady-state kinetics (Figures 1 and S1). ^bMeasured by the fluorescence assay (Figure 3B). ^cCalculated as described at the Experimental Section, using eq 5 and data from Table 3.

Mg^{2+} Binds to ecTSase and Affects the Affinities of Both Substrates to the Protein. Mg^{2+} can affect the activity of an enzyme by either chelating with the substrate to form a more active Mg–substrate complex or binding to the protein to alter its conformations and/or constitute the active site.⁵ To determine the functional role of Mg^{2+} in TSase activity, we measured the values of dissociation constant (K_d) that describe the interactions between Mg^{2+} and apo-ecTSase, between Mg^{2+} and the binary ecTSase–dUMP complex, and between Mg^{2+} and the covalent ternary complex ecTSase–(SF–dUMP)– CH_2H_4fol . The binary and ternary complexes resemble the intermediates B and C, respectively, in the catalyzed reaction (Scheme 1).⁵⁵ The K_d values were determined to be 27 ± 7 mM for apo-ecTSase, 0.5 ± 0.2 M for ecTSase–dUMP, and 3.7 ± 1.2 mM for ecTSase–(SF–dUMP)– CH_2H_4fol , respectively (Figure 3A,C). The relative magnitudes of these K_d values suggest the activation effect is most likely induced by Mg^{2+} binding to the ternary enzyme complex rather than the binary complex. This finding is in accordance with Mg^{2+} binding at the folate binding site rather than chelating with dUMP.

To investigate the effects of Mg^{2+} on the interactions between the substrates and enzyme, we measured the dissociation constants for dUMP (K_d^{dUMP}) binding to apo-ecTSase and to the ecTSase– Mg^{2+} complex, using the fluorescence assay (Figure 3B). We also assessed the

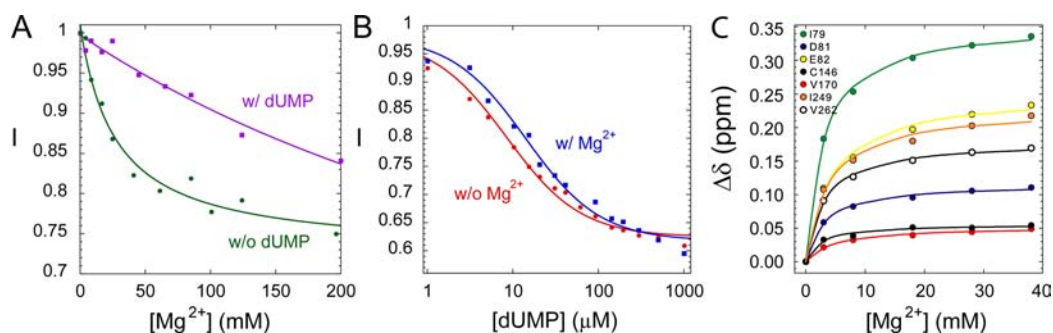


Figure 3. Fluorescence intensity (I , relative to the initial intensity) of ecTSase (A) vs MgCl_2 concentration in the absence (w/o, green) and presence of $100 \mu\text{M}$ (w/, purple) dUMP and (B) vs dUMP concentration in the absence (w/o, red) and presence of 50 mM (w/, blue) of MgCl_2 . (C) Changes in backbone chemical shifts as Mg^{2+} is titrated into the solution of ecTSase–(5F-dUMP)– $\text{CH}_2\text{H}_4\text{fol}$ complex. Different colors represent seven representative residues. The detailed data analysis is provided in the Experimental Section.

Table 3. Observed H/D KIEs on k_{cat} ($^Dk_{\text{cat}}$) and Intrinsic H/D KIEs (Dk) on the Hydride Transfer of ecTSase at $25 \text{ }^\circ\text{C}$, in the Absence (w/o) and Presence (w/) of 50 mM MgCl_2

$6R\text{-}^3\text{H-CH}_2\text{H}_4\text{fol}$	k_{cat} (s^{-1})	$K_{\text{M}}^{\text{CH}_2\text{H}_4\text{fol}}$ (μM)	$K_{\text{T}}^{\text{CH}_2\text{H}_4\text{fol}}$ (mM)	$^Dk_{\text{cat}}$	Dk	
w/ Mg^{2+}	$^x\text{H}=\text{H}$	8.7 ± 0.2	15 ± 1	0.76 ± 0.07	3.8 ± 0.3	3.9 ± 0.2^a
	$^x\text{H}=\text{D}$	2.3 ± 0.2	19 ± 5	3 ± 1		
w/o Mg^{2+}				3.7 ± 0.1^b	3.8 ± 0.3^c	

^aDetermined from the competitive KIE experiment (Table S2, $25 \text{ }^\circ\text{C}$). ^bFrom ref 20. ^cFrom ref 26.

dissociation constants for $\text{CH}_2\text{H}_4\text{fol}$ ($K_{\text{d}}^{\text{CH}_2\text{H}_4\text{fol}}$) binding to the ecTSase–dUMP and ecTSase–dUMP– Mg^{2+} complexes,⁵⁶ using the equation derived by Klinman and Matthews⁵⁷ (eq 5). The presence of Mg^{2+} increased the $K_{\text{d}}^{\text{dUMP}}$ value (Table 2), which is consistent with the increase of $K_{\text{M}}^{\text{dUMP}}$ and implicates the same effects on binding and productive binding of the substrate dUMP. On the contrary, the presence of Mg^{2+} decreased the $K_{\text{d}}^{\text{CH}_2\text{H}_4\text{fol}}$ value (Table 2), suggesting that Mg^{2+} ameliorates the interaction between $\text{CH}_2\text{H}_4\text{fol}$ and the enzyme. The unchanged $K_{\text{M}}^{\text{CH}_2\text{H}_4\text{fol}}$ value is probably due to the compensating effects of decrease in $K_{\text{d}}^{\text{CH}_2\text{H}_4\text{fol}}$ and increase in the hydride-transfer rate constant with Mg^{2+} (k_{cat} is a parameter at the nominator of the $K_{\text{M}}^{\text{CH}_2\text{H}_4\text{fol}}$ term).⁵⁸ The higher affinity of $\text{CH}_2\text{H}_4\text{fol}$ in the presence of Mg^{2+} corroborates the reduction of ΔTS^\ddagger found in the steady-state kinetic experiments above, since the binding of $\text{CH}_2\text{H}_4\text{fol}$ induces large conformational changes of TSase that close the active-site cavity and properly align the reactants for catalysis.^{24,25} Therefore, our kinetic and binding studies suggest that Mg^{2+} stabilizes the bound $\text{CH}_2\text{H}_4\text{fol}$ and thus reduces the entropic cost for the conformational changes of the protein that lead to formation of the reactive complexes, thereby accelerating k_{cat} .

Mg^{2+} Affects the Rate but not the Intrinsic KIE of Hydride Transfer. Previous studies suggested that the hydride transfer is rate limiting for k_{cat} of ecTSase in the absence of Mg^{2+} .²⁰ To examine if Mg^{2+} changes the rate-limiting step for the catalytic turnover, we measured the intrinsic KIE as well as the KIE on k_{cat} with $6R\text{-}^3\text{H-CH}_2\text{H}_4\text{fol}$ ($^x\text{H}=\text{H}$, D, or T) at $25 \text{ }^\circ\text{C}$ in the presence of 50 mM MgCl_2 (Figure S2). The observed KIE on k_{cat} ($^Dk_{\text{cat}}$) is equal to the intrinsic KIE (Table 3), indicating that the hydride transfer is also rate limiting for k_{cat} in the presence of Mg^{2+} . Therefore, the observed effects on k_{cat} and the activation energy parameters (Figure 2 and Table 1) suggest that Mg^{2+} accelerates the rate of the hydride transfer and slightly reduces the entropy of activation on this step.

To investigate the effects of Mg^{2+} on the TRS of the hydride transfer, we determined the temperature dependence of the intrinsic KIE. We measured the observed KIEs on the second-

order rate constant $k_{\text{cat}}/K_{\text{M}}^{\text{CH}_2\text{H}_4\text{fol}}$ (simplified as $k_{\text{cat}}/K_{\text{M}}$ hereafter)^{51,59} and used Northrop's method to extract the intrinsic KIEs as described before.²⁶ In the absence of Mg^{2+} , the observed KIEs are similar to the intrinsic values (Figure 4A),

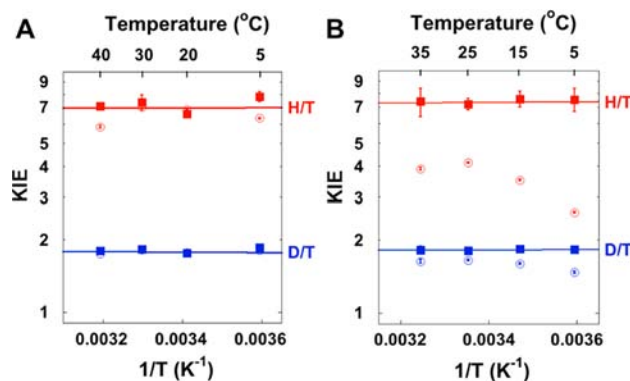


Figure 4. Observed KIEs on $k_{\text{cat}}/K_{\text{M}}$ (empty symbols) and the intrinsic KIEs (filled symbols) on the hydride transfer in the (A) absence and (B) presence of 50 mM MgCl_2 . Figure A is adopted from ref 26 with permission from ACS. The observed and intrinsic KIE values in the presence of Mg^{2+} are presented in Table S2. The lines are nonlinear regression of the intrinsic KIEs to Arrhenius equation (eq 9).

implying that the hydride transfer is also (at least partially) rate limiting for $k_{\text{cat}}/K_{\text{M}}$.²⁶ On the contrary, the observed KIEs are smaller than the intrinsic KIEs in the presence of Mg^{2+} (Figure 4B), indicating that the hydride transfer is no longer rate-limiting for $k_{\text{cat}}/K_{\text{M}}$. This observation agrees with the accelerated rate of hydride transfer by Mg^{2+} and suggests a larger kinetic commitment (C_{f} in Table S2) for $k_{\text{cat}}/K_{\text{M}}$.^{50,51} However, the intrinsic KIE on the hydride transfer has the same value as measured in the absence of Mg^{2+} and remains temperature independent (Figure 4 and Table 4). Based on the Marcus-like model, these observations suggest that Mg^{2+}

Table 4. Isotope Effects on the Arrhenius Parameters of the Hydride Transfer of ecTSase in the Absence (w/o) and Presence (w/) of 50 mM MgCl₂^a

	w/o Mg ²⁺ ^b	w/Mg ²⁺
A_H/A_T	6.8 ± 2.8	6.6 ± 1.3
$\Delta E_{a, H-T}$ (kcal/mol)	0.02 ± 0.25	-0.06 ± 0.12

^aThe intrinsic KIE values were fit to eq 9, where A_H/A_T is the isotope on the Arrhenius prefactors, and $\Delta E_{a, H-T}$ is the difference in the activation energies of the hydride transfer between the hydrogen and tritium. ^bFrom ref 26.

facilitates protein motions that bring the hydride donor in CH₂H₄fol into proximity with its acceptor in dUMP (i.e., pre- and reorganization), but it does not alter the TRS of the hydride transfer.

Structural and Dynamic Effects of Mg²⁺ Binding to ecTSase. It is generally difficult to discriminate Mg²⁺ from a water molecule in X-ray diffraction data, due to the similarity between their electron densities. The main difference between water and Mg²⁺ is the tetrahedral coordination of the first and octahedral coordination of the latter. To investigate the structural origin for our observed kinetic effects, we carefully examined a number of previously solved crystal structures for putative Mg²⁺ ions that were octahedrally coordinated via shorter hydrogen bonds (H-bonds) with surrounding water molecules or oxyanions of the protein. A 1.3 Å-resolution crystal structure²⁷ of ecTSase ternary complex with dUMP and a cofactor analogue, 10-propargyl-5,8-dideazafolic acid

(CB3717), shows such geometry for water 1092 at the binding cleft for the glutamyl (Glu) tail of CB3717 (Figure 5A, PDB ID: originally 2G8O and now 4IW5). The glutamate side chain of CB3717 forms H-bonds with a cluster of water molecules with octahedral “water 1092” at its base (Figure 5A). Although some magnesium might be present, the crystal of this TSase–dUMP–CB3717 complex was grown against 1.4 M sodium citrate, thus this “water 1092” is most likely a Na⁺ ion. As Na⁺ is isoelectronic to Mg²⁺, has the same size, and also has octahedral coordination geometry, this Na⁺ binding site could also accommodate Mg²⁺ with a similar geometry. We also determined another ternary complex of ecTSase with dUMP and a di-Glu antifolate inhibitor (BGC 945, now known as ONX 0801) that was crystallized with 0.2 M MgCl₂.⁶⁰ While this crystallization condition resulted in lower resolution than the one with sodium citrate (1.75⁶⁰ vs 1.3 Å²⁷), it shows unambiguous electron density for an octahedrally hydrated Mg²⁺ (Figure S5, PDB ID 4ISK). The Mg²⁺ site in the ecTSase complex with BGC945 and the possible Mg²⁺ site in the ecTSase ternary complex with CB3717 are different, owing to the different stereochemistry of each inhibitor’s Glu moiety; however in both cases the cation establishes H-bond interactions between the Glu moiety and an electronegative protein loop and stabilizes this interface through electrostatic interactions (Figures 5 and S5). We also used NMR chemical shift changes to map the Mg²⁺ binding site in the ecTSase–(5F-dUMP)–CH₂H₄fol complex (Figure 5B,C) and found excellent agreement between the binding sites identified in the crystal structures and in solution. The protein loop that Mg²⁺

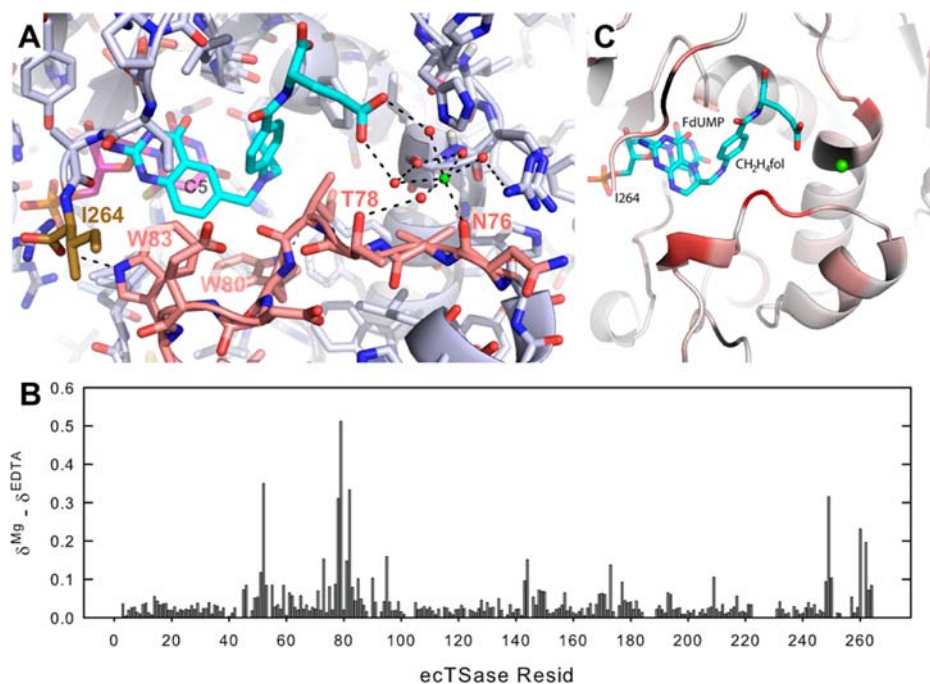


Figure 5. (A) Octahedral cation (green) binds to the surface of the ecTSase complex with dUMP (magenta) and CB3717 (cyan) (PDB ID 4IW5). All the catalyzed chemical transformations occur near C5 of dUMP (labeled in black, see Scheme 1) in the interior active site. Mg²⁺ mediates an H-bond network between the Glu-tail of the cofactor and an electrophilic part of a loop (residues 76–93 in ecTSase, pink) containing residues W80 and W83, which are important for closing the active site cavity (see text). The C-terminus (I264, brown) is very flexible in apo-TSase, but it is immobilized by an H-bond with W83 in the ternary complex upon the cofactor binding. (B) Difference in backbone amide chemical shift upon Mg²⁺ binding to the ecTSase complex with 5F-dUMP and CH₂H₄fol. (C) NMR data from panel B are painted onto the crystal structure of the corresponding complex (PDB ID 1TSN) using a white to red color scheme representing zero to maximum chemical shift changes. Prolines and unassigned residues are colored black. The binding site of Mg²⁺ (green) suggested from panel A is indicated in this structure by aligning 1TSN with 4IW5.

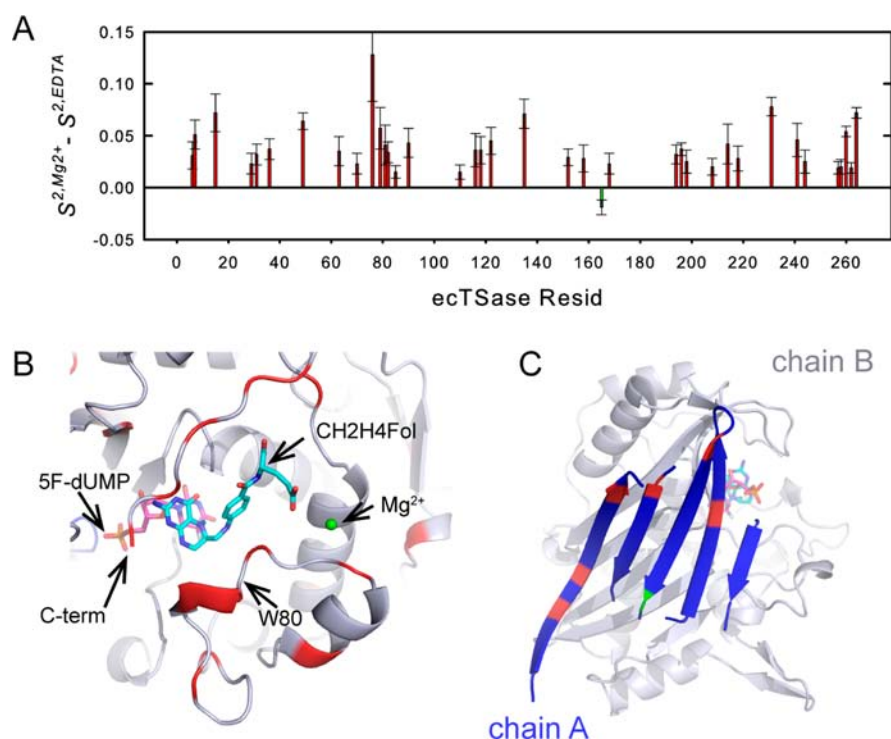


Figure 6. (A) Mg^{2+} binding rigidifies the ecTSase–(SF-dUMP)– $\text{CH}_2\text{H}_4\text{fol}$ complex. Significant ($>2\sigma$) differences in ^{15}N – ^1H order parameters ($\Delta S^2 = S^2, \text{Mg}^{2+} - S^2, \text{EDTA}$, see Experimental Section) are shown, where positive ΔS^2 indicates rigidification in the Mg^{2+} -bound complex on the ps–ns time scale. S^2 data for the two individual states are shown in Figure S4. (B) Residues that become more rigid upon Mg^{2+} binding are highlighted in red on a ternary complex structure. Residues with no significant change are colored gray, and the single bond vector that becomes more flexible is not visible in this view. The suggested binding site for Mg^{2+} is shown in green. (C) Mg^{2+} binding also affects dynamics at the dimer interface. Significant changes in S^2 are highlighted on the five-stranded β -sheet of one subunit (chain A) that comprises the dimer interface. Rigidified residues are colored in red, and Q165 (which becomes more flexible) is colored in green.

interacts with is involved in closing the active site upon cofactor binding.^{24,25} Particularly, W83 on this loop forms an H-bond with the C-terminal carboxylic group (residue I264 in ecTSase) as $\text{CH}_2\text{H}_4\text{fol}$ binds to the protein, which helps to immobilize the C-terminus to seal the active site cavity. This loop also contains W80, which not only orients L143 to protect the active site from bulk solvent but also forms an H-bond with E58, while E58 coordinates the active site water molecules essential for TSase activity.^{25,32}

Our kinetic and binding studies above suggest that Mg^{2+} accelerates k_{cat} by reducing the entropic cost for the conformational changes of the protein that accompanies progression from the ground state to TRS. To investigate the effects of Mg^{2+} on the protein flexibility, we conducted NMR relaxation experiments to measure the generalized order parameters (S^2) for backbone ^{15}N – ^1H vectors in the ecTSase–(SF-dUMP)– $\text{CH}_2\text{H}_4\text{fol}$ complex in the absence and presence of Mg^{2+} (see Experimental Section and Figure S4). S^2 represents the rigidity of the structure, which ranges from 0 to 1 indicating complete disorder to fixed bond orientation on the ps–ns time scale.^{61,62} Importantly, S^2 has been shown to be an excellent proxy for conformational entropy in a number of systems.^{63–68} In our experiments, 37 bond vectors exhibited significant ($>2\sigma$) differences in S^2 upon Mg^{2+} binding, of which 36 showed elevated S^2 (Figure 6A). This is consistent with a model in which Mg^{2+} binding lowers the entropic barrier of the hydride transfer by paying some of the conformational entropy penalty in the ground state. Although we cannot measure S^2 for the TRS to evaluate differences in the protein flexibility in that

state, our KIE experiments above suggest that Mg^{2+} does not affect the TRS (Figure 4). In addition, Mg^{2+} binding rigidifies regions that stabilize the closed conformation of the enzyme (e.g., C-terminus and the loop containing W80 and W83, Figure 6A,B), which corroborates the indications from the X-ray crystallographic data above. Lastly, it is notable that dynamic effects extend beyond the metal binding region, as distal bond vectors, including some at the dimer interface (I29, G31, F36, F152, K158, Q165, and D198), show significant changes (Figure 6C).

Taken together, our kinetic, structural, and NMR data suggest that the weak binding of Mg^{2+} to the surface of TSase stabilizes the closed conformations of the ternary enzyme complex, which not only enhances the affinity of $\text{CH}_2\text{H}_4\text{fol}$ but also increases the fraction of reactive complexes for the chemical reactions after $\text{CH}_2\text{H}_4\text{fol}$ binding. A similar relay between the protein surface and the active site has been observed for the TSase domain of the bifunctional TSase-dihydrofolate reductase enzyme in *Cryptosporidium hominis*. In that case, two nonconserved residues that bind the Glu-tail of $\text{CH}_2\text{H}_4\text{fol}$ are responsible for the faster k_{cat} of this TSase domain than other TSase enzymes.⁶⁹ Mutations on those two residues affected the positioning and flexibility of the cofactor, and this effect propagated into the active site and reduced k_{cat} of the TSase domain.⁷⁰

The binding site of Mg^{2+} revealed by the current study agrees with previous observations that Mg^{2+} modulated the selective inhibition of poly-Glu antifolates toward bacterial and viral TSase activities.⁵² The binding region for the poly-Glu moiety

is not conserved among different species⁷¹ and is also quite open to solvent, which would allow Mg²⁺ to bind and modulate H-bonds at several locations between the poly-Glu tail and the protein loop (Figure 5). The residues in the loop of ecTSase whose side chains contribute to the Mg²⁺-mediated H-bond network include T78 in both ternary complexes and E82 in the di-Glu inhibitor complex. The corresponding residues in human TSase are lysine and alanine, respectively. These differences may preclude formation of analogous Mg²⁺-mediated H-bond network between human TSase and the cofactor, explaining the lack of sensitivity of human TSase activity to Mg²⁺. Future studies can exploit our current findings and design species-specific TSase inhibitors, such as antifolates with a poly-Glu substitute that would create a perfect binding site for Mg²⁺ in a specific TSase enzyme, which may lead to species-specific drugs that target DNA biosynthesis.

CONCLUSIONS

The role of protein motions in the chemical reactions catalyzed by enzymes has been a subject of great contemporary interest. Experimental and computational studies of dihydrofolate reductase, for example, have suggested a “network of coupled motions” to rationalize long-range structural and dynamic effects of remote residues on the catalyzed reaction.^{43,72–75} It is interesting to examine this concept in more complex enzymatic systems, such as TSase. TSase exploits progressive conformational changes to assist the binding and orientation of ligands and to accommodate structural changes in the ligands during the catalyzed chemical transformations.^{24,25} Particularly, our recent study of Y209W ecTSase demonstrated that protein motions at various time scales can affect different parameters of the catalyzed hydride transfer step.¹⁹ The current study has explored how Mg²⁺ weakly bound at the protein surface affects the kinetics of wild-type ecTSase through long-range interactions throughout the enzyme. Our crystal structures suggest a binding site for Mg²⁺ near the Glu moiety of the cofactor, which stabilizes the closed conformations of the ternary enzyme complex of ecTSase. Our kinetic findings suggest that the binding of Mg²⁺ reduces the entropic cost for protein conformational changes that lead to formation of the reactive complexes and thereby accelerates the rate of hydride transfer. NMR-derived order parameters, which are a proxy for conformational entropy, support this hypothesis. While the hydride transfer is faster and is no longer rate limiting in the presence of Mg²⁺, the intrinsic KIE and its temperature dependence are unchanged, suggesting that Mg²⁺ binding does not affect the TRS of the hydride transfer. Since TSase is crucial for DNA replication, these results agree with previously established positive correlation between the intracellular magnesium content and proliferating rate of *E. coli* cells.^{7,8} Future studies will continue to incorporate structural and kinetic experiments to better define the Mg²⁺ binding site and specificity and clarify its effect on TSase catalysis. The possible effect of other biologically relevant divalent metals will also be explored. Most importantly, comparison studies between the human and bacterial TSases may reveal the origin of their different sensitivity to Mg²⁺ in the kinetics. Understanding those differences can assist in designing species-specific antibiotic drugs by exploiting the interaction between Mg²⁺ and nonconserved residues of bacterial TSases.

EXPERIMENTAL SECTION

Materials and Instruments. [2-¹⁴C] dUMP (specific radioactivity 53 Ci/mol) was purchased from Moravak Biochemicals. [6R-³H]-CH₂H₄folate (³H = D or T) was synthesized according to our published procedure,¹⁹ and unlabeled CH₂H₄folate (³H=H) was a generous gift from EPROVA (Switzerland). Ultima gold liquid scintillation cocktail reagent was purchased from Packard Bioscience. Liquid scintillation vials were purchased from Research Products International Corp. The ecTSase enzymes were expressed and purified according to the established procedures.⁷⁶ All other materials were purchased from Sigma. The steady-state kinetic experiments were conducted using a Hewlett-Packard Model 8452A diode-array spectrophotometer equipped with a temperature-controlled cuvette assembly. For the competitive KIE experiments, the radioactive materials were separated with an Agilent Technologies model 1100 HPLC system with a Supelco Discovery C18 reverse phase column and analyzed with a liquid scintillation counter. Figures 5B and 6A were generated with SigmaPlot 10.0, Figures 5A,C and 6B,C were generated with Pymol v1.5.0.4,⁷⁷ and all other figures with Kaleida-Graph (version 4.03).

Experiments and Data Analysis. Steady-State Kinetic Experiments. Our previous experiments measured the steady-state initial velocities of ecTSase in the absence of Mg²⁺ by monitoring the increase of absorbance at 340 nm that indicates conversion of CH₂H₄fol to dihydrofolate ($\Delta\epsilon_{340\text{ nm}} = 6.4\text{ mM}^{-1}\text{ cm}^{-1}$).²⁶ In the current study, we conducted the same experiments in the presence of 50 mM MgCl₂. Addition of ecTSase to a final concentration of 20 nM (concentration in terms of dimer, same below) initiated the reaction. Values of k_{cat} and K_{M} of CH₂H₄fol were measured with 100 μM dUMP at 5, 15, 25, and 35 °C, and the K_{M} value of dUMP was measured with 150 μM CH₂H₄fol at 25 °C. To check the potential effects of ionic strength on the activity of TSase, we also conducted the control experiment at 25 °C, in which MgCl₂ was replaced by 50 mM CaCl₂, and found no effects on the initial velocities.

Analysis of Steady-State Initial Velocities. Analysis of the initial velocities at each temperature employed the least-squares nonlinear regression available in KaleidaGraph (version 4.03). The initial velocities of ecTSase vs concentration of dUMP can be fit with the standard Michaelis–Menten equation. In contrast, high concentrations of CH₂H₄fol inhibit the activity of ecTSase, and the data were analyzed by the general equation for uncompetitive substrate inhibition (eq 2), which incorporates Hill coefficients to account for the potential cooperativity in substrate binding.⁷⁸

$$\frac{v}{[E]_{\text{t}}} = \frac{k_{\text{cat}} + k_{\text{cat}(i)} \left(\frac{[S]}{K_{\text{i}}} \right)^x}{1 + \left(\frac{K_{\text{M}}}{[S]} \right)^n + \left(\frac{[S]}{K_{\text{i}}} \right)^x} \quad (2)$$

where $[E]_{\text{t}}$ is the total enzyme concentration, $[S]$ is the concentration of the substrate (e.g., CH₂H₄fol in this case), $k_{\text{cat}(i)}$ accounts for the activity when the substrate binds in the inhibitory mode (if products can still form when the substrate binds in the inhibitory mode); K_{M} and K_{i} are the Michaelis constant and inhibition constant of the substrate, respectively, and n and x are Hill coefficients for the cooperativity of substrate binding in the productive and inhibitory mode, respectively. Previous crystallographic studies suggested that the alternate binding mode of CH₂H₄fol is unproductive due to improper orientation for the catalyzed reaction, i.e., $k_{\text{cat}(i)} = 0$.⁵⁴ Analysis of the initial velocities using eq 2 with $k_{\text{cat}(i)} = 0$ shows that the integer value of $n = 1$ provides the best fit in both the absence and presence of Mg²⁺. This result agrees with the previously suggested “half-of-the-sites” activity for ecTSase, i.e., one competent active site per dimer with no cooperativity in the productive binding mode ($n = 1$).^{21–23} To reduce errors on the kinetic parameters in the statistical analysis, we fixed $n = 1$ in the following data analysis, which simplifies eq 2 to eq 3:

$$\frac{v}{[E]_{\text{t}}} = \frac{k_{\text{cat}}[S]}{K_{\text{M}} + [S] \left(1 + \left(\frac{[S]}{K_{\text{i}}} \right)^x \right)} \quad (3)$$

Analysis of the initial velocities using eq 3 shows that the integer value of $x = 2$ provides the best fit in the absence of Mg^{2+} , while $x = 1$ is optimal in the presence of Mg^{2+} . These results imply that Mg^{2+} alters the interaction between the protein and CH_2H_4fol , which eliminates the cooperativity of CH_2H_4fol binding in the inhibitory mode. Further analysis on the kinetic parameters used $x = 2$ for the initial velocities in the absence of Mg^{2+} and $x = 1$ in the presence of Mg^{2+} , and the results are presented in Figure 1 and Table S1.

Equilibrium Dissociation Constants. Fluorescence Assay. Equilibrium dissociation constants of the enzyme complexes were measured by titrating Mg^{2+} or dUMP into a solution of ecTSase, following the previously established fluorescence assay.²⁰ The excitation wavelength was 290 nm, and the maximum emission of fluorescence was at 334 nm. Each experiment contained at least a duplicate of data sets. To correct for fluorescence changes that are not associated with the protein, we conducted parallel titrations in which ecTSase was replaced by a quantity of tryptophan with the same initial fluorescence intensity. We also conducted control experiments in which dUMP was titrated into the solution that contained all the reagents except the protein/tryptophan in the absence and presence of Mg^{2+} . The control experiments did not produce detectable changes in fluorescence signals, suggesting that the interactions between the ligands (if exist) do not affect the fluorescence intensity measured for the protein.

Binding of Mg^{2+} . We measured the dissociation constants that describe the interactions between Mg^{2+} and ecTSase apoenzyme and between Mg^{2+} and the binary ecTSase–dUMP complex. The initial solution contained 25 mM dithiothreitol (DTT), 1 mM ethylenediaminetetraacetate (EDTA), and 0.8 μ M ecTSase preincubated with 0 or 100 μ M dUMP at 25 °C in 100 mM tris(hydroxymethyl)aminomethane (Tris)/HCl buffer (pH 7.5). Titrating a concentrated solution of $MgCl_2$ into the initial solution caused a decrease in protein fluorescence (after correcting for the dilution factor), which indicates protein conformational changes induced by Mg^{2+} binding. Although Mg^{2+} can possibly bind into multiple sites of TSase, we fit the data to the simplest model (i.e., one-site binding, eq 4) to compare the affinity of this ion for the apoenzyme and the binary complex:

$$I = \frac{I_E K_d + I_{EL}[L]}{K_d + [L]} \quad (4)$$

where I is the observed fluorescence intensity, I_E and I_{EL} are the molar fluorescence intensities for the apoenzyme and binary complex, respectively, $[L]$ is the ligand concentration, and K_d is the dissociation constant for L.

Binding of dUMP (K_d^{dUMP}). We also measured the dissociation constants that describe the interactions between dUMP and apoenzyme and between dUMP and the binary ecTSase– Mg^{2+} complex. The initial solution contained 25 mM DTT, 1 mM EDTA, and 0.8 μ M ecTSase preincubated with 0 or 50 mM $MgCl_2$ in 100 mM Tris/HCl buffer (pH 7.5). Titrating a concentrated solution of dUMP into the initial solution caused a decrease in protein fluorescence due to dUMP binding. Previous studies suggested dUMP only binds to one active site per ecTSase dimer in the absence of CH_2H_4fol .²⁰ Thus, we fit the data to the one-site binding model (eq 4) to evaluate the dissociation constants of dUMP.

Binding of CH_2H_4fol ($K_d^{CH_2H_4fol}$). Due to nonspecific quenching of fluorescence by formaldehyde (HCHO), which is used to stabilize CH_2H_4fol in solution, we cannot directly measure the dissociation constant of CH_2H_4fol by the fluorescence assay. Instead, we used the equation derived by Klinman and Matthews⁵⁷ (eq 5) to calculate the dissociation constants of CH_2H_4fol :

$$K_d = K_M \frac{D(k_{cat}/K_M)_H - 1}{Dk_{cat} - 1} \quad (5)$$

where K_M is obtained from the steady-state kinetic experiments (Table S1), Dk_{cat} is H/D KIE measured on k_{cat} by the noncompetitive KIE experiment (Table 3), and $D(k_{cat}/K_M)_H$ is the H/D KIE on k_{cat}/K_M , which is calculated from the intrinsic H/D KIE and kinetic commitment factor on the hydride transfer (Table S2).

NMR Titration Experiments. We used NMR spectroscopy to measure the K_d for Mg^{2+} binding to the ecTSase–(SF-dUMP)– CH_2H_4fol complex. Resonance assignments for the metal-free complex are deposited in the BMRB (accession 19082) and are described elsewhere.⁷⁹ $MgCl_2$ was titrated into the ternary complex, and the chemical shift changes of backbone amide groups were monitored by TROSY 1H – ^{15}N HSQC spectra. It is important to note that only one set of resonances is observed in HSQC spectra, which indicates symmetric binding of SF-dUMP and CH_2H_4fol to both active sites of the homodimer. The initial solution contained 0.5 mM ecTSase–FdUMP– CH_2H_4fol , 25 mM HEPES, 100 mM NaCl, 10 mM TCEP-HCl, 0.01% NaN_3 , pH 7.5. Chemical shift changes in both 1H and ^{15}N were taken into account based on eq 6:

$$\Delta\delta = \sqrt{0.1 * \Delta\delta(^{15}N)^2 + \Delta\delta(^1H)} \quad (6)$$

A K_d value for each resolved resonance showing a change in chemical shift upon Mg^{2+} addition was obtained by fitting $\Delta\delta$ to eq 7:

$$\Delta\delta = \Delta\delta_{max} \frac{\{K_D + [L_T] + [E_T] - \sqrt{(K_D + [L_T] + [E_T])^2 - 4[L_T][E_T]}\}}{2[E_T]} \quad (7)$$

where $[L_T]$ and $[E_T]$ are the total Mg^{2+} and ecTSase concentrations, respectively. The reported K_d of 3.7 ± 1.2 mM represents the mean and standard deviation of the fits from 29 separate amide resonances.

Noncompetitive KIE Experiments. Spencer et al. have measured the KIEs on k_{cat} at 25 °C using the noncompetitive experiments in the absence of Mg^{2+} .²⁰ We conducted the experiments under the same conditions in the presence of 50 mM $MgCl_2$, with 100 μ M dUMP and various concentrations of 6R- 3H - CH_2H_4fol ($^3H = H$ or D) in 100 mM Tris/HCl buffer (pH 7.5). Addition of ecTSase to the final concentration of 20 or 80 nM initiated the reaction for 6R- H - CH_2H_4fol or 6R- D - CH_2H_4fol , respectively.

Competitive KIE Experiments. Our previous study used the competitive method to measure the KIEs on k_{cat}/K_M and the temperature dependence of intrinsic KIE on the hydride transfer step in the absence of Mg^{2+} .²⁶ In the current study, we conducted the experiments under the same conditions in the presence of 50 mM $MgCl_2$. Following the previously published procedure,²⁶ we used the modified Northrop method to extract the intrinsic KIE from the observed H/T and D/T KIEs on k_{cat}/K_M (eq 8).^{45,50,51}

$$\frac{T(k_{cat}/K_M)_H^{-1} - 1}{T(k_{cat}/K_M)_D^{-1} - 1} = \frac{(T_k)^{-1} - 1}{(T_k)^{-1/3.34} - 1} \quad (8)$$

where $T(k_{cat}/K_M)_H$ and $T(k_{cat}/K_M)_D$ are the observed H/T and D/T KIEs on k_{cat}/K_M , respectively, and T_k is the intrinsic H/T KIE on the hydride transfer ($T_k = k_H/k_T$). We have developed an online program, as well as a Mathematica script, to solve eq 8 numerically for T_k at each temperature (<http://chem.uiowa.edu/kohen-research-group/tools.html>). Fitting the intrinsic KIE values to the Arrhenius equation (eq 9) allows analysis of their temperature dependence.⁴⁵

$$T(k)_L = \frac{k_L}{k_T} = \frac{A_L}{A_T} \exp\left(\frac{\Delta E_a}{RT}\right) \quad (9)$$

where the subscripts L and T denote the light (H or D) and heavy (T) isotopes of hydrogen, respectively, and ΔE_a is the difference in the activation energies of the hydride transfer between the light and heavy isotopes. Since the hydride transfer is irreversible, the comparison between the observed and intrinsic KIEs provides the forward kinetic commitment (C_f) on k_{cat}/K_M (eq 10).^{50,51} Table S2 summarizes the observed and intrinsic KIEs, as well as C_f at the four experimental temperatures in the presence of Mg^{2+} .

$$T(k_{\text{cat}}/K_M)_H = \frac{T_k + C_f}{1 + C_f}$$

$$\Rightarrow C_f = \frac{T_k - T(k_{\text{cat}}/K_M)_H}{(k_{\text{cat}}/K_M)_H - 1} \quad (10)$$

Similarly, for H/D KIEs,

$$D(k_{\text{cat}}/K_M)_H = \frac{D_k + C_f}{1 + C_f} \quad (11)$$

Equation 11 was used to calculate the H/D KIE on k_{cat}/K_M at 25 °C from D_k and C_f (Table S2).

Identifying Mg^{2+} in the Crystal Structures. Divalent Mg^{2+} ion has an identical number of electrons (10) as water and thus is difficult to distinguish in electron-density maps, particularly if the position is partially occupied or the maps are obtained at low resolution. We examined the water molecules in a 1.3 Å-resolution crystal structure of the ternary ecTSase-dUMP-CB3717 complex (PDB ID: 2G8O) for putative Mg^{2+} ions with an approximate octahedral arrangement of hydrogen bonding partners. A few candidate water molecules were on the periphery of the protein outside the binding region for the ligands, while the only candidate water (i.e., putative Mg^{2+}) that can potentially affect catalysis was in the binding groove for the Glu-moiety of the cofactor (Figure 5A, new PDB ID: 4IWS). This putative Mg^{2+} formed H-bonds with five other water molecules and with the backbone carbonyl of N76. Interatomic distances of five of the H-bonds were 2.4 Å, and the sixth was 2.7 Å, which are shorter than the average H-bond length between water molecules. Two of the coordinated water molecules formed H-bonds with the carboxyl oxygen of the Glu of the cofactor, while four of them (including one water that was also H-bonded with the cofactor Glu) formed H-bonds with the protein backbone carbonyl or side chains (Figure 5A). This water cluster was only seen in the more highly resolved protomer (i.e., with lower isotropic B-factors) of the ecTSase dimer. Since this crystal was grown against 1.4 M sodium citrate, this putative Mg^{2+} is most likely a Na^+ ion. In contrast, the electron density map for both protomers of the ecTSase ternary complex (PDB ID 4ISK) with dUMP and a di-Glu antifolate inhibitor (BGC945) has strong, unambiguous density for Mg^{2+} that is octahedrally coordinated with six water molecules in the poly-Glu binding sites (Figure S5).⁶⁰ This density can be fit with the ideal geometry for an octahedrally coordinated Mg^{2+} , where the distances between Mg^{2+} and coordinated water molecules are ~2.1 Å.

NMR Spin Relaxation.⁷⁹ Backbone dynamics were assessed using TROSY versions of ^{15}N R_1 , $R_{1\rho}$, and $\{^1H\}$ - ^{15}N heteronuclear NOE pulse sequences.⁸⁰ Data were collected at 500 and 600 MHz on Bruker Avance III spectrometers equipped with TCI cryogenic probeheads. For the metal free complex, the conditions were 0.5 mM ecTSase-FdUMP- CH_2H_4fol , 25 mM $NaPO_4$, 150 mM NaCl, 1 mM EDTA, 10 mM DTT, pH 7.5, 298 K. For the Mg^{2+} -bound complex, the conditions were 0.5 mM ecTSase-FdUMP- CH_2H_4fol , 25 mM HEPES, 50 mM NaCl, 40 mM $MgCl_2$, 10 mM TCEP-HCl, pH 7.5, 298 K. HEPES was used in the presence of Mg^{2+} due to the low solubility product of magnesium phosphate. In the absence of metal, HSQC spectra were identical in HEPES vs phosphate and DTT vs TCEP-HCl. ^{15}N R_1 data were collected with the fids interleaved using relaxation delays of 0, 400, 800, 1600, 2400, and 3200 ms (the underlined time points were measured twice for error estimation). ^{15}N $R_{1\rho}$ data were also collected with the fids interleaved using relaxation delays of 1, 5, 10, 20, 30, 50, and 70 ms. The strength of the spin-lock field was 1.4 kHz. R_1 and $R_{1\rho}$ decay rates were fit to peak intensities using expfit2 (in-house written software). Pure R_2 rates were obtained from R_1 and $R_{1\rho}$ rates as described previously.⁸⁰ The raw relaxation rates are plotted in Figure S3.

We used TENSOR2⁸¹ in conjunction with PDB ID 1TSN to select the optimal global tumbling models. The best fit isotropic global tumbling times were 29 and 31 ns/rad for the metal-free and metal-bound complexes, respectively. However, for both the Mg^{2+} -bound and metal-free cases, an axially symmetric anisotropic model was chosen based on statistical criteria. Model selection and data fitting

were carried out as described before.⁸² Model-free order parameters are shown in Figure S4.

■ ASSOCIATED CONTENT

● Supporting Information

Steady state initial velocities vs dUMP concentrations; initial velocities vs concentration of $6R\text{-}^3H\text{-}CH_2H_4fol$ ($^3H = H$ or D); steady-state kinetic parameters; the KIE and C_f values at different temperatures; raw ^{15}N R_1 , R_2 , and $\{^1H\}$ - ^{15}N heteronuclear NOE spin relaxation data; and NMR order parameters; table with data collection and refinement statistics; and a figure that shows the binding site of Mg^{2+} in the ecTSase complex with BGC945. This material is available free of charge via the Internet at <http://pubs.acs.org>.

■ AUTHOR INFORMATION

Corresponding Author

amnon-kohen@uiowa.edu

Present Addresses

¹Department of Biochemistry, Albert Einstein College of Medicine, Bronx, NY 10461

[#]Ensign, United States Navy, Goose Creek, SC 29445

Notes

The authors declare no competing financial interest.

■ ACKNOWLEDGMENTS

This work was supported by NIH GM065368 (A.K.), NIH GM083059 (A.L.L.), NIH GM51232 (R.M.S.). Z.W. was also supported by a fellowship from the University of Iowa Center for Biocatalysis and Bioprocessing and by activities of the Predoctoral Training program in Biotechnology, NIH grant 2T32GM008365.

■ REFERENCES

- (1) Dokmanic, I.; Sikic, M.; Tomic, S. *Acta Crystallogr., Sect. D* **2008**, *64*, 257–263.
- (2) Harding, M. M.; Nowicki, M. W.; Walkinshaw, M. D. *Crystallogr. Rev.* **2010**, *16*, 247–302.
- (3) Saris, N. E.; Mervaaala, E.; Karppanen, H.; Khawaja, J. A.; Lewenstam, A. *Clin. Chim. Acta* **2000**, *294*, 1–26.
- (4) Romani, A. M.; Scarpa, A. *Front Biosci.* **2000**, *5*, D720–D734.
- (5) Cowan, J. A. *Biomaterials* **2002**, *15*, 225–235.
- (6) Wolf, F. I.; Fasanella, S.; Tedesco, B.; Torsello, A.; Sgambato, A.; Faraglia, B.; Palozza, P.; Boninsegna, A.; Cittadini, A. *Front Biosci.* **2004**, *9*, 2056–2062.
- (7) Moncany, M. L.; Kellenberger, E. *Experientia* **1981**, *37*, 846–847.
- (8) Chang, C. F.; Shuman, H.; Somlyo, A. P. *J. Bacteriol.* **1986**, *167*, 935–939.
- (9) Perry, K. M.; Fauman, E. B.; Finer-Moore, J. S.; Montfort, W. R.; Maley, G. F.; Maley, F.; Stroud, R. M. *Proteins* **1990**, *8*, 315–333.
- (10) Carreras, C. W.; Santi, D. V. *Annu. Rev. Biochem.* **1995**, *64*, 721–762.
- (11) Pozzi, C.; Ferrari, S.; Cortesi, D.; Luciani, R.; Stroud, R. M.; Catalano, A.; Costi, M. P.; Mangani, S. *Acta Crystallogr., Sect. D* **2012**, *68*, 1232–1241.
- (12) Shen, C. J.; Liu, Y. J.; Lu, C. P. *J. Virol.* **2012**, *86*, 10900.
- (13) Colson, P.; Gimenez, G.; Boyer, M.; Fournous, G.; Raoult, D. *PLoS ONE* **2011**, *6*, e18935.
- (14) Johnston, P. G.; Lenz, H. J.; Leichman, C. G.; Danenberg, K. D.; Allegra, C. J.; Danenberg, P. V.; Leichman, L. *Cancer Res.* **1995**, *55*, 1407–1412.
- (15) Chen, C.-Y.; Chang, Y.-L.; Shih, J.-Y.; Lin, J.-W.; Chen, K.-Y.; Yang, C.-H.; Yu, C.-J.; Yang, P.-C. *Lung Cancer* **2011**, *74*, 132–138.
- (16) Costi, M. P. *Med. Res. Rev.* **1998**, *18*, 21–42.

- (17) Longley, D. B.; Johnston, P. G. In *Apoptosis, Cell Signaling, and Human Diseases: Molecular Mechanisms*; Srivastava, R., Ed.; Humana Press: New York, 2007; Vol. 1, pp 263–278.
- (18) Costi, M. P.; Tondi, D.; Rinaldi, M.; Barlocco, D.; Pecorari, P.; Soragni, F.; Venturelli, A.; Stroud, R. M. *Biochim. Biophys. Acta* **2002**, *1587*, 206–214.
- (19) Wang, Z.; Abeysinghe, T.; Finer-Moore, J. S.; Stroud, R. M.; Kohen, A. *J. Am. Chem. Soc.* **2012**, *134*, 17722–17730.
- (20) Spencer, H. T.; Villafranca, J. E.; Appleman, J. R. *Biochemistry* **1997**, *36*, 4212–4222.
- (21) Maley, F.; Pedersenlane, J.; Changchien, L. M. *Biochemistry* **1995**, *34*, 1469–1474.
- (22) Anderson, A. C.; O'Neil, R. H.; DeLano, W. L.; Stroud, R. M. *Biochemistry* **1999**, *38*, 13829–13836.
- (23) Saxl, R. L.; Changchien, L. M.; Hardy, L. W.; Maley, F. *Biochemistry* **2001**, *40*, 5275–5282.
- (24) Stroud, R. M.; Finer-Moore, J. S. *Biochemistry* **2003**, *42*, 239–247.
- (25) Finer-Moore, J. S.; Santi, D. V.; Stroud, R. M. *Biochemistry* **2003**, *42*, 248–256.
- (26) Agrawal, N.; Hong, B.; Mihai, C.; Kohen, A. *Biochemistry* **2004**, *43*, 1998–2006.
- (27) Newby, Z.; Lee, T. T.; Morse, R. J.; Liu, Y.; Liu, L.; Venkatraman, P.; Santi, D. V.; Finer-Moore, J. S.; Stroud, R. M. *Biochemistry* **2006**, *45*, 7415–7428.
- (28) Wang, Z.; Kohen, A. *J. Am. Chem. Soc.* **2010**, *132*, 9820–9825.
- (29) Kanaan, N.; Roca, M.; Tunon, I.; Marti, S.; Moliner, V. *J. Phys. Chem. B* **2010**, *114*, 13593–13600.
- (30) Kanaan, N.; Roca, M.; Tunon, I.; Marti, S.; Moliner, V. *J. Phys. Chem. Chem. Phys.* **2010**, *12*, 11657–11664.
- (31) Kanaan, N.; Ferrer, S.; Marti, S.; Garcia-Viloca, M.; Kohen, A.; Moliner, V. *J. Am. Chem. Soc.* **2011**, *133*, 6692–6702.
- (32) Wang, Z.; Ferrer, S.; Moliner, V.; Kohen, A. *Biochemistry* **2013**.
- (33) Bandaria, J. N.; Cheatum, C. M.; Kohen, A. *J. Am. Chem. Soc.* **2009**, *131*, 10151–10155.
- (34) Kohen, A.; Cannio, R.; Bartolucci, S.; Klinman, J. P. *Nature* **1999**, *399*, 496–499.
- (35) Sikorski, R. S.; Wang, L.; Markham, K. A.; Rajagopalan, P. T.; Benkovic, S. J.; Kohen, A. *J. Am. Chem. Soc.* **2004**, *126*, 4778–4779.
- (36) Fan, F.; Gadda, G. *J. Am. Chem. Soc.* **2005**, *127*, 17954–61.
- (37) Nagel, Z. D.; Klinman, J. P. *Chem. Rev.* **2010**, *110*, PR41–PR67.
- (38) Pudney, C. R.; Johannissen, L. O.; Sutcliffe, M. J.; Hay, S.; Scrutton, N. S. *J. Am. Chem. Soc.* **2010**, *132*, 11329–11335.
- (39) Borgis, D. C.; Lee, S. Y.; Hynes, J. T. *Chem. Phys. Lett.* **1989**, *162*, 19–26.
- (40) Kuznetsov, A. M.; Ulstrup, J. *Can. J. Chem.* **1999**, *77*, 1085–1096.
- (41) Marcus, R. A. *J. Chem. Phys.* **2006**, *125*, 194504.
- (42) Marcus, R. A. *J. Phys. Chem. B* **2007**, *111*, 6643–6654.
- (43) Hammes, G. G.; Benkovic, S. J.; Hammes-Schiffer, S. *Biochemistry* **2011**, *50*, 10422–10430.
- (44) Hay, S.; Scrutton, N. S. *Nat. Chem.* **2012**, *4*, 161–168.
- (45) Wang, Z.; Roston, D.; Kohen, A. *Adv. Protein Chem. Struct. Biol.* **2012**, *87*, 155–180.
- (46) Warshel, A. *J. Biol. Chem.* **1998**, *273*, 27035–27038.
- (47) Cannon, W. R.; Benkovic, S. J. *J. Biol. Chem.* **1998**, *273*, 26257–60.
- (48) Rajagopalan, P. T.; Benkovic, S. J. *Chem. Rec.* **2002**, *2*, 24–36.
- (49) Hammes-Schiffer, S.; Benkovic, S. J. *Annu. Rev. Biochem.* **2006**, *75*, 519–541.
- (50) Northrop, D. B. *Biochemistry* **1975**, *14*, 2644–2651.
- (51) Cook, P. F.; Cleland, W. W. In *Enzyme Kinetics and Mechanism*; Garland Science: London ; New York, 2007, p 253–324.
- (52) Maley, G. F.; Maley, F.; Baugh, C. M. *J. Biol. Chem.* **1979**, *254*, 7485–7.
- (53) Rode, W.; Jastreboff, M. M. *Mol. Cell. Biochem.* **1984**, *60*, 73–76.
- (54) Birdsall, D. L.; Finer-Moore, J.; Stroud, R. M. *J. Mol. Biol.* **1996**, *255*, 522–535.
- (55) Hyatt, D. C.; Maley, F.; Montfort, W. R. *Biochemistry* **1997**, *36*, 4585–4594.
- (56) Since the bound dUMP in the active site elaborates a large hydrophobic surface to accommodate cofactor binding, ecTase binds dUMP and CH₂H₄fol sequentially (refs 24 and 25).
- (57) Klinman, J. P.; Matthews, R. G. *J. Am. Chem. Soc.* **1985**, *107*, 1058–1060.
- (58) Cook, P. F.; Cleland, W. W. In *Enzyme Kinetics and Mechanism*; Garland Science: London, New York, 2007, pp 35–58.
- (59) Kohen, A.; Roston, D.; Stojković, V.; Wang, Z. In *Encyclopedia of Analytical Chemistry*; Meyers, R. A., Ed.; John Wiley & Sons, Ltd: Chichester, U.K., 2011; Vol. S1-S3, pp 77–99.
- (60) Tochowicz, A.; Dalziel, S.; Eidam, O.; O'Connell, J. D., 3rd; Griner, S.; Finer-Moore, J. S.; Stroud, R. M. *J. Med. Chem.* **2013**, submitted.
- (61) Lipari, G.; Szabo, A. *J. Am. Chem. Soc.* **1982**, *104*, 4559–4570.
- (62) Lipari, G.; Szabo, A. *J. Am. Chem. Soc.* **1982**, *104*, 4546–4559.
- (63) Popovych, N.; Sun, S.; Ebright, R. H.; Kalodimos, C. G. *Nat. Struct. Mol. Biol.* **2006**, *13*, 831–838.
- (64) Frederick, K. K.; Marlow, M. S.; Valentine, K. G.; Wand, A. J. *Nature* **2007**, *448*, 325–329.
- (65) Marlow, M. S.; Dogan, J.; Frederick, K. K.; Valentine, K. G.; Wand, A. J. *Nat. Chem. Biol.* **2010**, *6*, 352–358.
- (66) Tzeng, S. R.; Kalodimos, C. G. *Nature* **2012**, *488*, 236–240.
- (67) Wand, A. J. *Curr. Opin. Struct. Biol.* **2013**, *23*, 75–81.
- (68) Petit, C. M.; Zhang, J.; Sapienza, P. J.; Fuentes, E. J.; Lee, A. L. *Proc. Natl. Acad. Sci. U.S.A.* **2009**, *106*, 18249–18254.
- (69) Doan, L. T.; Martucci, W. E.; Vargo, M. A.; Atreya, C. E.; Anderson, K. S. *Biochemistry* **2007**, *46*, 8379–8391.
- (70) Martucci, W. E.; Vargo, M. A.; Anderson, K. S. *Biochemistry* **2008**, *47*, 8902–8911.
- (71) Kamb, A.; Finer-Moore, J.; Calvert, A. H.; Stroud, R. M. *Biochemistry* **1992**, *31*, 9883–9890.
- (72) Agarwal, P. K.; Billeter, S. R.; Rajagopalan, P. T.; Benkovic, S. J.; Hammes-Schiffer, S. *Proc. Natl. Acad. Sci. U.S.A.* **2002**, *99*, 2794–2799.
- (73) Wong, K. F.; Selzer, T.; Benkovic, S. J.; Hammes-Schiffer, S. *Proc. Natl. Acad. Sci. U.S.A.* **2005**, *102*, 6807–6812.
- (74) Nashine, V. C.; Hammes-Schiffer, S.; Benkovic, S. J. *Curr. Opin. Chem. Biol.* **2010**, *14*, 644–651.
- (75) Wang, L.; Goodey, N. M.; Benkovic, S. J.; Kohen, A. *Proc. Natl. Acad. Sci. U.S.A.* **2006**, *103*, 15753–15758.
- (76) Changchien, L.-M.; Garibian, A.; Frasca, V.; Lobo, A.; Maley, G. F.; Maley, F. *Protein Expression Purif.* **2000**, *19*, 265–270.
- (77) Pymol, v1.5.0.4; Schrodinger, LLC: New York, 2010.
- (78) LiCata, V. J.; Allewell, N. M. *Biophys. Chem.* **1997**, *64*, 225–234.
- (79) Sapienza, P. J.; Lee, A. L. *Biomol. NMR Assign.*, **2013**, in press.
- (80) Lakomek, N. A.; Ying, J.; Bax, A. *J. Biomol. NMR* **2012**, *53*, 209–221.
- (81) Dosset, P.; Hus, J. C.; Blackledge, M.; Marion, D. *J. Biomol. NMR* **2000**, *16*, 23–28.
- (82) Sapienza, P. J.; Mauldin, R. V.; Lee, A. L. *J. Mol. Biol.* **2011**, *405*, 378–394.

NOTE ADDED AFTER ASAP PUBLICATION

Corrections have been made to Equation 1, Table 3, the link listed in the paragraph between Equations 8 and 9, and Reference 56 in the version published ASAP on May 10, 2013. The corrected version was re-posted on May 13, 2013.